REPORT DOCUMENTATION PAGE

Form Approved
OMB No. 0704-0188

1. AGENCY USE ONLY (Leave blank)	2. REPORT DATE	3. REPORT TYPE AND DATES COVERED
	09/01/98	

4. TITLE AND SUBTITLE

Promoting Atomic Scale Engineering by Quantifying Experimental Observations of Dislocation Cores

5. FUNDING NUMBERS

6. AUTHOR(S)

Kevin J. Hemker

7. PERFORMING ORGANIZATION NAME(S) AND ADDRESS(ES)

Johns Hopkins University
Mechanical Engineering Department
3400 N. Charles St., 200 Latrobe Hall
Baltimore, MD 21218

8. PERFORMING ORGANIZATION REPORT NUMBER

F49620-95-1-0280

9. SPONSORING / MONITORING AGENCY NAME(S) AND ADDRESS(ES)

Air Force Office of Scientific Research
Bolling AFB, DC 20332-6448

10. SPONSORING / MONITORING AGENCY REPORT NUMBER

11. SUPPLIMENTARY NOTES

12a. DISTRIBUTION / AVAILABILITY STATEMENT

Approved for public release;
distribution unlimited.

12b. DISTRIBUTION CODE

13. ABSTRACT *(Maximum 200 words)*

Intermetallic alloys are excellent materials for bridging the gap between atomic level processes and macroscopic properties, because the mechanical behavior of these alloys can be closely related to their dislocation structures. The research support by this grant, and described here, was undertaken to elucidate the relationship between atomic level dislocation core structures, alloy composition, and macroscopic mechanical behavior in a series of (Nix,Fe1-x)3Ge alloys and to develop the techniques necessary to perform microsample tensile tests of single crystalline intermetallic alloys. The results from this study, which are described below, have resulted in 6 journal articles, 5 conference proceedings, numerous conference presentations and two M.S. Dissertations. The dislocation structure observations provide benchmarks for first-principle electronic structure calculations and the availability of microsample testing allows for mesoscale testing of individual grains in a number of structural alloys. Both have proven to be valuable tools for bridging the length scales that govern the mechanical performance of high temperature structural materials.

14. SUBJECT TERMS

15. NUMBER OF PAGES
17

16. PRICE CODE

17. SECURITY CLASSIFICATION OF REPORT	18. SECURITY CLASSIFICATION OF THIS PAGE	19. SECURITY CLASSIFICATION OF ABSTRACT	20. LIMITATION OF ABSTRACT
Unclassified	Unclassified	Unclassified	Unclassified

WU

FINAL REPORT

Project Title:

PROMOTING ATOMIC SCALE ENGINEERING BY QUANTIFYING EXPERIMENTAL OBSERVATIONS OF DISLOCATION CORES

AFOSR Grant No: F49620-95-1-0280

Duration: April 1, 1996 - March 31, 1998

Principal Investigator: Associate Professor Kevin J. Hemker
Department of Mechanical Engineering
The Johns Hopkins University
Baltimore, MD 21218-2686
Tel: (410) 516-4489
Fax: (410) 516-7254
E-mail: hemker@jhu.edu

Submitted to:
AIR FORCE OFFICE OF SCIENTIFIC RESEARCH
Attn: Dr. Spencer Wu
Chemistry and Materials Sciences Directorate
Bolling AFB, Washington DC 20332-6448

REPORT DOCUMENTATION PAGE

AFRL-SR-BL-TR-98-
0453

1. AGENCY USE ONLY (Leave blank)	2. REPORT DATE	3. REPC
	09/01/98	

4. TITLE AND SUBTITLE

Promoting Atomic Scale Engineering by Quantifying Experimental Observations of Dislocation Cores

5. FUNDING NUMBERS

6. AUTHOR(S)

Kevin J. Hemker

7. PERFORMING ORGANIZATION NAME(S) AND ADDRESS(ES)

Johns Hopkins University
Mechanical Engineering Department
3400 N. Charles St., 200 Latrobe Hall
Baltimore, MD 21218

8. PERFORMING ORGANIZATION REPORT NUMBER

F49620-95-1-0280

9. SPONSORING / MONITORING AGENCY NAME(S) AND ADDRESS(ES)

Air Force Office of Scientific Research
Bolling AFB, DC 20332-6448

10. SPONSORING / MONITORING AGENCY REPORT NUMBER

11. SUPPLIMENTARY NOTES

12a. DISTRIBUTION / AVAILABILITY STATEMENT

Approved for public release;
distribution unlimited.

12b. DISTRIBUTION CODE

13. ABSTRACT *(Maximum 200 words)*

Intermetallic alloys are excellent materials for bridging the gap between atomic level processes and macroscopic properties, because the mechanical behavior of these alloys can be closely related to their dislocation structures. The research support by this grant, and described here, was undertaken to elucidate the relationship between atomic level dislocation core structures, alloy composition, and macroscopic mechanical behavior in a series of (Nix,Fe1-x)3Ge alloys and to develop the techniques necessary to perform microsample tensile tests of single crystalline intermetallic alloys. The results from this study, which are described below, have resulted in 6 journal articles, 5 conference proceedings, numerous conference presentations and two M.S. Dissertations. The dislocation structure observations provide benchmarks for first-principle electronic structure calculations and the availability of microsample testing allows for mesoscale testing of individual grains in a number of structural alloys. Both have proven to be valuable tools for bridging the length scales that govern the mechanical performance of high temperature structural materials.

14. SUBJECT TERMS

15. NUMBER OF PAGES
17

16. PRICE CODE

17. SECURITY CLASSIFICATION OF REPORT	18. SECURITY CLASSIFICATION OF THIS PAGE	19. SECURITY CLASSIFICATION OF ABSTRACT	20. LIMITATION OF ABSTRACT
Unclassified	Unclassified	Unclassified	Unclassified

§ EXECUTIVE SUMMARY

Intermetallic alloys are excellent materials for bridging the gap between atomic level processes and macroscopic properties, because the mechanical behavior of these alloys can be closely related to their dislocation structures. The research supported by this grant, and described here, was undertaken to elucidate the relationship between atomic level dislocation core structures, alloy composition, and macroscopic mechanical behavior in a series of $(Ni_xFe_{1-x})_3Ge$ alloys and to develop the techniques necessary to perform microsample tensile tests of single crystalline intermetallic alloys. The results from this study, which are described below, have resulted in 6 journal articles, 5 conference proceedings, 12 conference presentations and two M.S. Dissertations. The dislocation structure observations provide benchmarks for first-principle electronic structure calculations and the availability of microsample testing allows for mesoscale testing of individual grains in a number of structural alloys. Both have proven to be valuable tools for bridging the length scales that govern the mechanical performance of high temperature structural materials.

1 TECHNICAL ACCOMPLISHMENTS :

1.1 Structure – property relations in $(Ni_xFe_{1-x})_3Ge$ alloys

Six alloys for the $(Ni_xFe_{1-x})_3Ge$ project have been obtained through collaboration with Dr. Dimiduk's group in the Materials Laboratory at the Wright Patterson Air Force Base (WPAFB). These compositions were chosen in accordance with the Ni_3Ge-Fe_3Ge pseudo-binary phase diagram constructed by Suzuki *et al.* (*Acta Metall.*, **28**, 301, 1980), which predicts a continuous solid solution of $L1_2$ alloys for this system. The alloy compositions (in at%) chosen for this study are: $Ni_{75}Ge_{25}$, $Ni_{60}Fe_{15}Ge_{25}$, $Ni_{50}Fe_{25}Ge_{25}$, $Ni_{43}Fe_{32}Ge_{25}$, $Ni_{20}Fe_{55}Ge_{25}$, and $Fe_{75}Ge_{25}$. A considerable portion of the first year was spent in the preparation of these alloys, which were obtained in the arc-cast form and subsequently hot iso-statically pressed and heat treated (at WPAFB) in a flowing argon atmosphere (1200K for 5 days followed by a single phase anneal at 873K for 14 days). The heat treatment and subsequent quench were required to attain the desired $L1_2$ crystal structure. Differential thermal analysis, optical microscopy, and x-ray and electron diffraction techniques were used for identification of phases in the undeformed material. This verified that the majority phase in each alloy had the $L1_2$ structure, with the Fe-rich alloys containing small fractions of other Fe-rich ordered phases with the $D0_3$ and $D0_{19}$ structures. These observations are at variance with the above-mentioned paper where the authors had reported the existence of a single phase field for the entire composition range.

Compression testing of samples has been conducted over a wide range of temperatures (77 K to 750 K). Specimens were electro-discharge machined from the HIP'ed and heat treated ingots. Comprehensive results from mechanical testing are presented in fig. 1. This figure indicates the anomalous behavior of the 0.2% offset flow stress (nominally the yield stress) in the Ni-rich alloys, as well as the gradual decrease and eventual disappearance of the flow stress anomaly as the Fe content approaches 32at%. Binary $Ni_{75}Ge_{25}$ clearly exhibited the flow stress anomaly in the low temperature region, rising from 205 MPa at 77 K to 455 MPa at 300 K. $Ni_{60}Fe_{15}Ge_{25}$ also exhibited the anomaly, rising from 528 MPa at 77 K to 643 MPa at 600K,

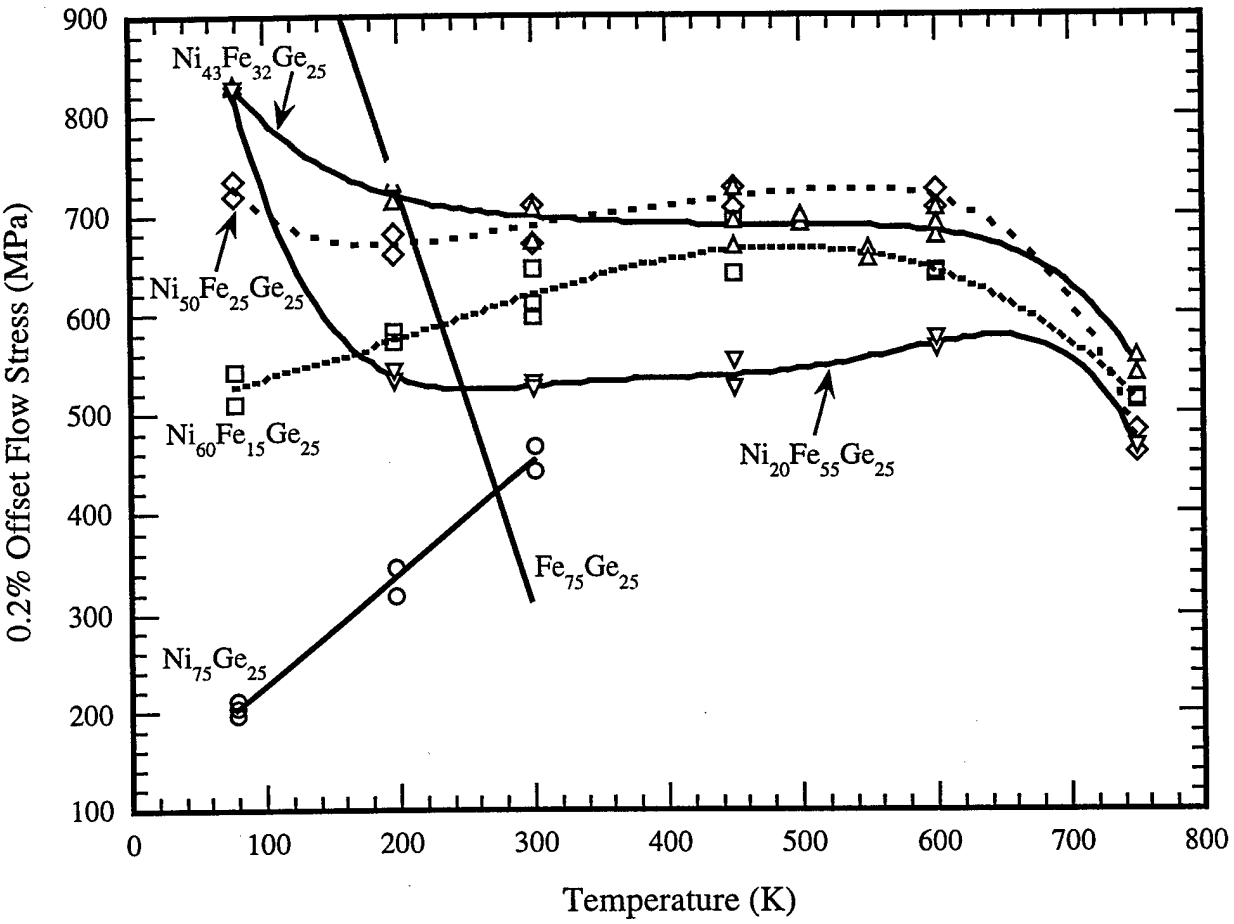

Fig. 1: Flow stress vs. temperature for the $(Ni_xFe_{1-x})_3Ge$ alloys, showing a transition from normal to anomalous behavior.

the peak temperature. The flow stress of $Ni_{50}Fe_{25}Ge_{15}$ almost exhibited a plateau, rising only from 671 MPa at 197K to 716 MPa at 600K. In contrast, the flow stress of $Ni_{43}Fe_{32}Ge_{25}$ showed a normal temperature dependence, decreasing monotonically as temperature was increased. As Fe content was further increased, the negative temperature dependence became much stronger, as shown by the dramatic drops in flow stress for $Ni_{20}Fe_{55}Ge_{25}$, and $Fe_{75}Ge_{25}$. Overall, an increase in Fe content appears to bring about a more normal temperature dependence of the flow stress.

TEM studies of the deformation microstructures have been performed in order to gain insight into the microscopic processes that control the macroscopic mechanical behavior described above. These observations are summarized in fig. 2, which shows the microstructures of the four Ni-rich alloys at various temperatures. The TEM observations indicate that the microstructure developed by $Ni_{75}Ge_{25}$ during deformation in the anomalous temperature regime is dominated by antiphase boundary (APB)-dissociated <110> superdislocations with narrow separations between the superpartial dislocations. Typically, systems of straight screw-oriented

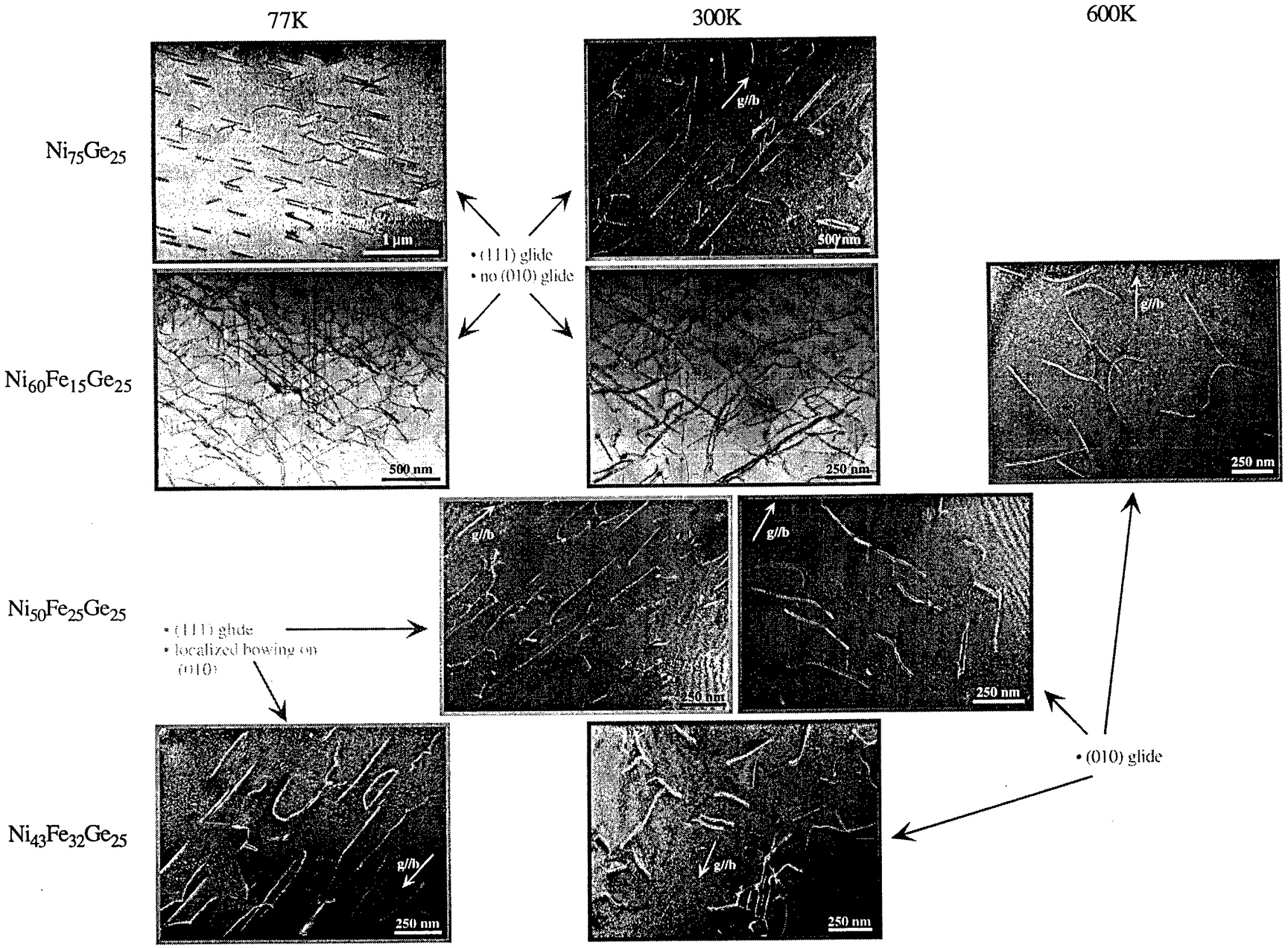

Fig. 2: Key observations of the deformation microstructures of the four Ni-rich alloys at various deformation temperatures. An increase in temperature or Fe content causes a transition from octahedral glide and cross-slip locking of screw-oriented superdislocations to cube glide of mixed superdislocations.

superdislocations were observed in the microstructure, suggesting the formation of Kear-Wilsdorf locks. In contrast, the microstructure of $Ni_{43}Fe_{32}Ge_{25}$ deformed at room temperature consisted almost exclusively of widely APB-dissociated and curved <110> superdislocations. Tilting experiments revealed that they were dissociated on the cube plane, an indication that cube glide had occurred. The occurrence of cube glide in $Ni_{43}Fe_{32}Ge_{25}$ is fundamentally different from the octahedral glide and cube cross-slip observed in $Ni_{75}Ge_{25}$. The differing mechanisms of dislocation motion coincide with different mechanical behavior exhibited by each alloy, i.e. octahedral glide is observed in anomalous $Ni_{75}Ge_{25}$, whereas cube glide is observed in normal $Ni_{43}Fe_{32}Ge_{25}$. The transition between these two mechanisms is well illustrated by the pair of micrographs for $Ni_{50}Fe_{25}Ge_{25}$, taken from separate grains within the same TEM foil, see fig. 2. In the first grain, screw superdislocations that lie on the cube plane have just begun to glide on the cube plane. The observation of switched-over kinks is indicative of an unlocking process. In contrast, the second grain shows mixed dislocations that have been gliding on the cube plane. It thus appears that superdislocations in $Ni_{50}Fe_{25}Ge_{25}$ undergo cube cross-slip and subsequent cube glide at ambient temperatures. The occurrence of both mechanisms for dislocation motion is coupled with a flow stress dependence in $Ni_{50}Fe_{25}Ge_{25}$ that shows only slight changes in flow stress between 77K and 600K. Overall, a transition from octahedral glide and cross-slip locking of screw superdislocations to cube glide of mixed superdislocations is seen to result from either an increase in Fe content or an increase in temperature. This transition to cube glide corresponds to a transition to normal temperature dependence of flow stress, i.e. disappearance of the flow stress anomaly.

Weak-beam TEM was used to characterize the separations of APB-dissociated superpartials. As illustrated in fig. 3, tilting experiments were performed in the TEM in order to determine the plane on which the APB was dissociated. When viewing along the normal to the dissociation plane, the widest and true separation is observed. In addition to determining the actual plane of dissociation, the true separation of the superpartials that bound the APB must be determined. Image shifts occur during weak-beam observations of narrowly dissociated superdislocations due to the overlapping strain fields of component superpartials. Correcting for these shifts to obtain the true equilibrium separation distances was performed within the framework of anisotropic elasticity using the computer simulation program CUFOUR (Schäublin and Stadelmann, *Mater. Sci. Eng.*, **A164**, 373, 1993). The corrected separation distances are listed in Table I. For each alloy at each deformation temperature, the dissociation of a particular superdislocation was measured; its line orientation/character and the plane on which it is dissociated are given in the third column of Table I. The fourth and fifth columns list the observed and corrected separation distances, while the sixth and seventh columns list APB energies calculated from the respective separations. It is seen that the {001} cube plane APB energy decreases much more significantly with increasing Fe content than does the {111} APB energy. Thus, the driving force for cube cross-slip rises sharply with Fe content.

A collaborative research project has been initiated with Professor Arthur Freeman of the Department of Physics, Northwestern University. Professor Freeman and Dr. Oleg Mryasov use first-principles calculations to generate the gamma (energy) surface associated with a complete dislocation as well as the dissociation scheme that is most favorable. In addition to dissociation

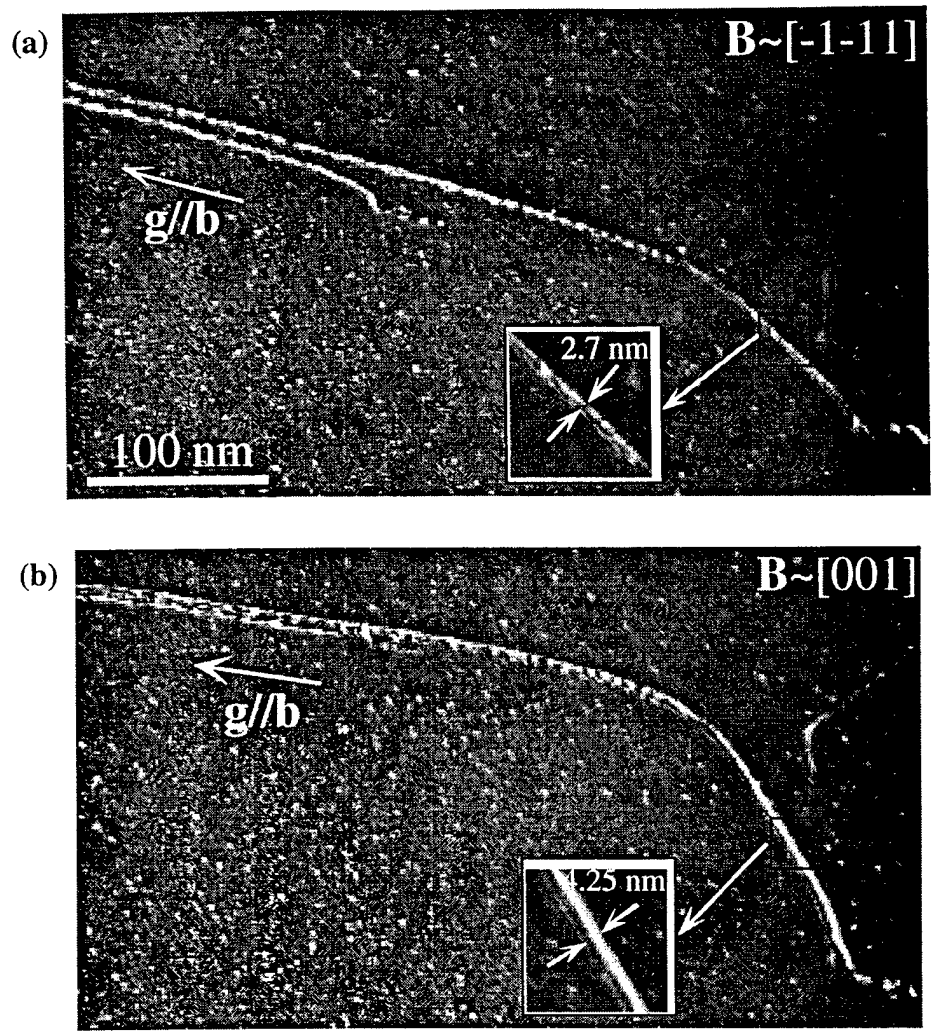

Fig. 3: An example of a TEM tilting experiment to determine the plane of dissociation for an APB in $Ni_{75}Ge_{25}$. (a) Viewed along an octahedral plane normal. (b) Viewed along a cube plane normal. The separation observed in (b) is wider than that in (a) or in any other direction, indicating that (b) is the true image of the dissociated APB.

schemes, the first-principles calculations can also yield fault energies and elastic constants. Dr. Mryasov has provided the single crystal elastic constants of Fe_3Ge and has also calculated the elastic constants of Ni_3Ge, which agree well with experimental values obtained using an ultrasonic resonance method. Linear interpolation between these values has allowed the elastic constants of the intermediate $(Ni_xFe_{1-x})_3Ge$ alloys to be determined. Modulus values obtained from the mechanical compression tests show good agreement with the polycrystalline elastic moduli that have been calculated from the elastic constants for each alloy. The agreement between the interpolated elastic constants and the experimentally determined moduli supports the validity of Dr. Mryasov's first-principles calculations. Moreover, since the interpolated elastic constants have been used in the computer simulations of the dissociation widths of superdislocations, this agreement increases confidence in the APB energies that have been obtained through the simulations.

Table I. Image shift corrections, with dissociation distances and calculated antiphase boundary energies in the Ni_3Ge–Fe_3Ge system as a function of alloy composition and temperature. The dissociation widths and in turn the fault energies have been corrected for image shifts within the framework of anisotropic elasticity.

Alloy Composition (Temperature)	Plane	Line Orientation	$d_{measured}$ (nm)	$d_{corrected}$ (nm)	Antiphase Boundary Energy (mJ/m^2)	
					$\gamma_{uncorrected}$	$\gamma_{corrected}$
$Ni_{75}Ge_{25}$	{001}	0°	3.8±0.4	2.7±0.1	212±22	296±11
(77K)	{111}	90°	5.5±0.2	3.6±0.3	220±8	339±29
	{111}	30°	3.5±0.2	2.7±0.2	259±15	337±25
$Ni_{75}Ge_{25}$	{001}	45°	4.2±0.2	3.7±0.2	261±13	292±12
(300K)	{001}	0°	3.7±0.5	2.7±0.2	219±29	297±22
$Ni_{60}Fe_{15}Ge_{25}$	{001}	0°	5.0±0.2	3.8±0.1	154±6	202±6
(77K)	{111}	90°	5.3±0.3	3.8±0.5	223±13	315±41
	{111}	60°	4.1±0.3	3.4±0.3	264±20	320±28
$Ni_{60}Fe_{15}Ge_{25}$	{001}	90°	8.9±0.3	8.2±0.2	141±5	153±4
(600K)	{001}	0°	6.2±0.2	5.5±0.3	124±4	140±7
$Ni_{50}Fe_{25}Ge_{25}$	{001}	90°	8.2±0.2	7.1±0.1	151±7	172±5
(300K)	{001}	0°	5.7±0.3	4.2±0.4	132±7	180±17
$Ni_{43}Fe_{32}Ge_{25}$	{001}	0°	5.8±0.3	5.4±0.3	127±5	132±8
(77K)	{111}	90°	6.8±0.3	4.2±0.2	168±7	272±13
$Ni_{43}Fe_{32}Ge_{25}$ (300K)	{001}	90°	12.9±0.4	9.0±0.3	95±3	137±4

The existence of a large difference in cube and octahedral plane APB energies is not the only factor governing cross-slip. Indeed, this difference cannot be used to explain the onset of cube glide in the $(Ni_xFe_{1-x})_3Ge$ system, as cube glide is first observed in $Ni_{50}Fe_{25}Ge_{25}$; although $Ni_{60}Fe_{15}Ge_{25}$ exhibits a large difference (130 mJ/m^2) in APB energies, no cube glide is observed in this alloy. The mobility of dislocations on the cube plane also plays a significant role in the transition to cube glide. Because the complex stacking fault (CSF) contained within a dissociated superpartial must lie on the octahedral plane, it provides Peierls-like resistance to motion on the cube plane. An increase in CSF energy or a corresponding decrease in CSF spacing would lead to increases in both cross-slip and cube glide. The CSF dissociations must therefore be determined in order to more fully characterize the core dissociations. Because the spacings between CSFs in a component superpartial are on the order of Ångstroms, resolving the separation will require high resolution electron microscopy (HREM), which is capable of resolving features below the nanometer length scale. Efforts are currently underway to couple first-principles calculations provided by Professor Freeman with HREM observations in order to accurately determine the CSF widths and hence the CSF energies. These values will complement the APB energies already determined and will allow a more complete understanding of the interrelationship between dislocation core dissociations and mechanical properties.

1.2 Microsample testing of single crystalline TiAl

Inspection of the Ti-Al phase diagram reveals that for aluminum contents near 56%, one passes directly from the liquid into the gamma phase field upon cooling from the melt. This provides a composition window in which single crystals of γ-TiAl may be grown. However, Bridgman and Czochralski crystal pulling methods cannot be used because of the high reactivity of the liquid phase of TiAl. Single crystals of Ti-55.5Al have been grown for this study using the optical float zone furnace at the University of Pennsylvania Laboratory for Research on the Structure of Matter. The optical float zone method provides a containerless growing environment, which is necessary for avoiding the introduction of impurities into the melt. In addition, the optical float zone furnace provides a means by which crystals may be seeded from bulk polycrystalline rods. Crystals of Ti-55.5Al 6-10 mm in diameter and 50 mm long were grown for this study.

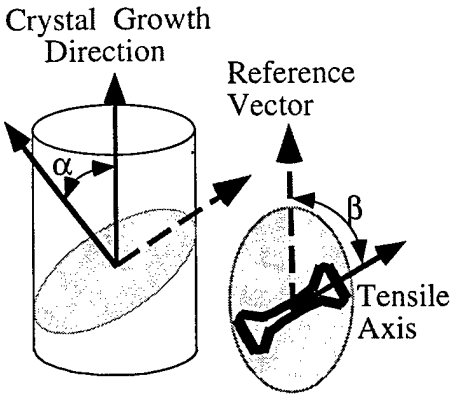

Fig. 4: Single Crystals of TiAl are cut into slices at prescribed angles, and microsamples are cut from these discs along desired orientations using a sinking EDM.

The lack of room temperature fracture toughness makes handling γ-TiAl very difficult, and this inherent fragility is compounded by the small size of the specimens. Conventional machining is prohibited by the brittle nature of the material, but electro-discharge machining (EDM) was found to be suitable for specimen cutting. The crystals were mounted and oriented in a double tilt 360• rotation goniometer and sliced at prescribed angles. Micro-samples were cut from these discs with a sinking EDM that was powered by a Micro-Fin controller, much in the way a cookie cutter is used to make cookies. See fig. 4 for a schematic of the orientation process. Samples that have been machined and are ready to be released for polishing are displayed in fig. 5. The preparation of microsamples in the manner described here facilitates mechanical testing in two ways. First, a large number of samples can be cut from a relatively small amount of

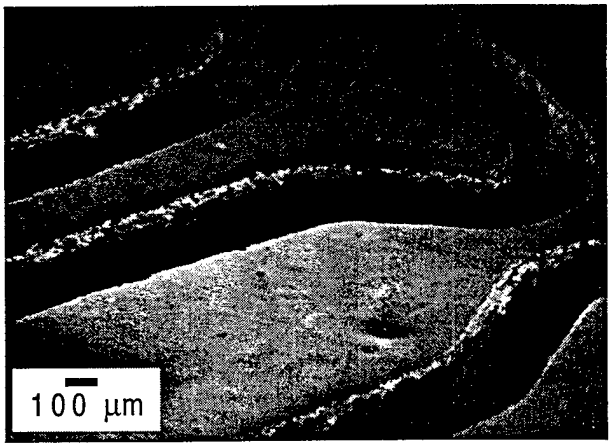

Fig. 5: SEM micrograph of a microsample just after being cut by the sinking EDM. The samples shown here are ready to be released and prepared for testing.

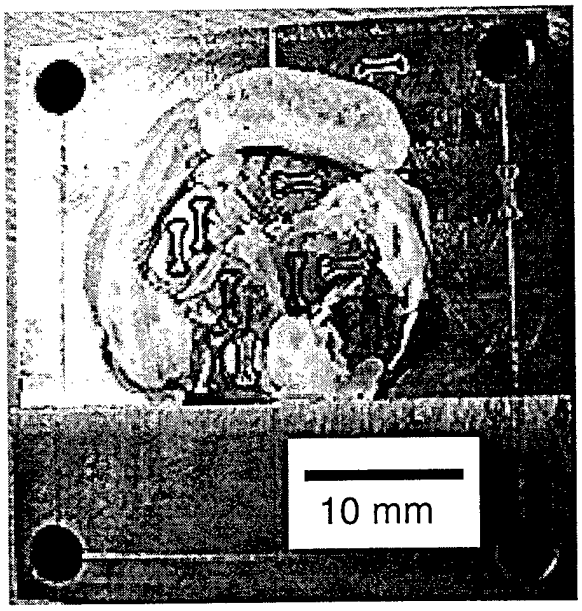

Fig. 6: Single crystal microsamples cut from individual grains of an ingot of Ti-52Al.

crystal. Second, the microsamples will allow us to test throughout the stereographic triangle and measure the resolved shear stress for both ordinary and superdislocation motion at a wide variety of orientations and temperatures.

As described earlier, single crystals of nominal composition near 56at% Al can be grown. It has been theorized that the mechanisms controlling deformation in this material may change as the composition of the alloy approaches the stoichiometric composition. To study the effect of composition on deformation, polycrystalline ingots of Ti-52Al and Ti-50Al have been overaged to enlarge the grain structure. Slices were cut from the ingot at desired thicknesses. The disks were polished and etched to reveal the grains. Grains that pass through the entire slice and were larger than microsamples were identified. Microsamples were EDM'd entirely out of one grain, resulting in single crystalline test specimens. A piece of an ingot that has had several single crystal samples machined from it is displayed in fig.6.

The as-cut samples were electro-polished to a mirror finish in a solution of 45% acetic acid, 45% butoxyethanol and 10% perchloric acid (by volume) at a temperature of -20 ^{0}C and voltage of 11.5 V. This electro-polishing removes the recast layer associated with the EDM and retains good edge quality on all four sides of the specimen. A cross-sectional view of a fractured microsample gage section is shown in fig. 7, and it is easy to see that a nearly rectangular cross-section is obtained. Mechanical polishing of the samples is possible, but is avoided for several reasons: the sides on the sample are extremely difficult to polish; mechanical polishing often introduces micro-cracks or flaws which lead to premature fracture of these extremely brittle specimens; the time and effort required to electro-polish a sample is less than mechanical polishing; and most importantly, the sample quality from electro-polishing has been found to be superior.

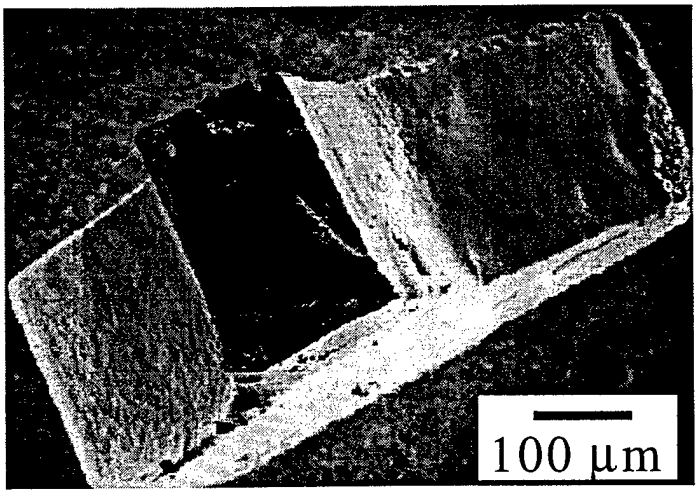

Fig. 7: Cross-sectional view of the gage section of a fractured microsample. This observation indicates that the rectangular cross-section is maintained and that the specimens are electro-polished to a mirror finish on all four sides.

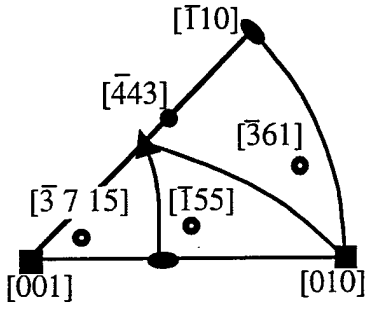

Fig. 8: The stereographic triangle showing the orientation of tension and compression samples that have been tested during this study.

Microsample specimens of single crystalline γ-TiAl have been tested along several different crystallographic directions. The loading axes have been chosen so that each of the three sections of the standard stereographic triangle are represented, see fig. 8. Results of three compression tests that were conducted at room temperature and orientations of [$\bar{4}$43], [$\bar{3}$61] and [$\bar{3}$ 7 15] are shown in fig. 9. The Young's moduli have been measured by averaging the data from a number of unload-reload curves (not shown) in the linear elastic portion of the tests, and the mean values for each orientation are reported in Table II. The 0.2% flow stress ($\sigma_{0.2\%}$) is denoted on the curves by dashed lines. The measured values of $\sigma_{0.2\%}$ have been multiplied by the appropriate Schmid factors, and the resolved shear stresses (RSS) for both ordinary (**b**=1/2<110]) and superlattice (**b**=<101]) dislocations are reported in Table II.

Microsample tensile tests have been conducted at several temperatures. Tensile testing at 300K was abandoned after several attempts ended with premature brittle fracture. High temperature testing is accomplished by placing a low voltage across the sample and driving a DC current through the specimen, which causes resistive heating of the microsample. Figure 9 displays the stress-strain curves that resulted from tensile tests performed at 500K. The Young's modulus was measured in the linear elastic portion of the curves and is reported in Table II. The

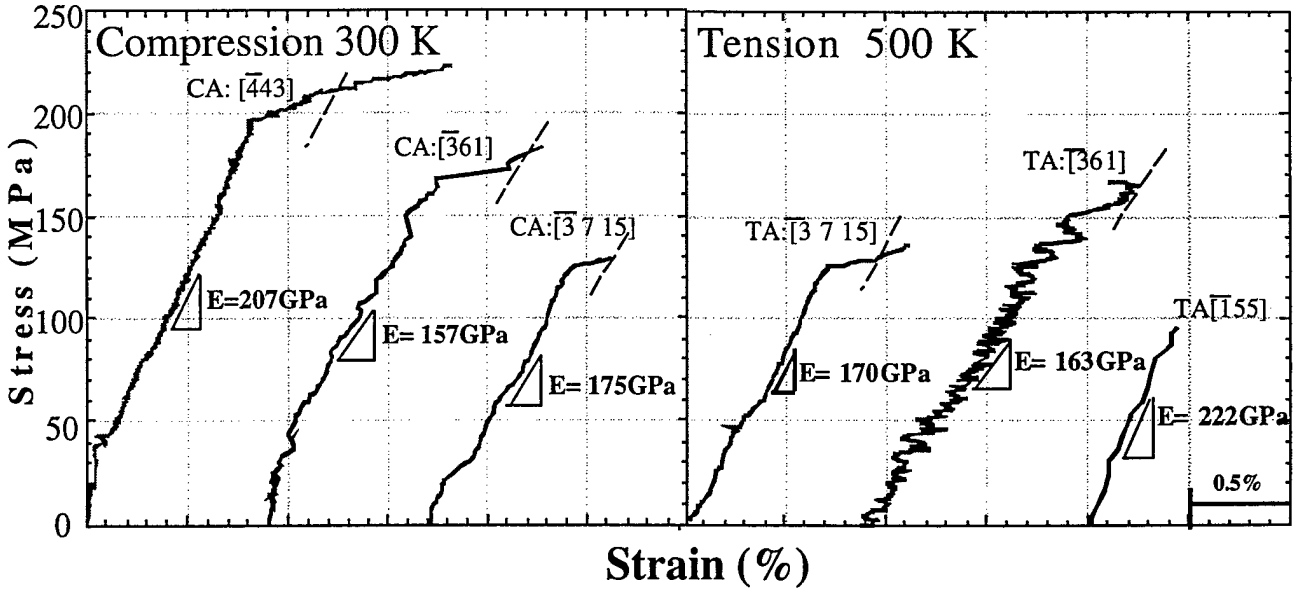

Fig. 9: Tension and compression stress-strain curves for γ-Ti-55.5Al single crystals deformed at 300K and 500K. The 0.2% offsets for the different orientations are given by the dotted lines. The [$\bar{1}$55] oriented sample fractured before yielding and no flow stress was measured, but values of $\sigma_{0.2\%}$ were obtained from the other orientations.

Table II: Measured and reference values of E (GPa), $\sigma_{0.2\%}$ (MPa) and RSS (MPa) for TiAl.

Loading Axis	$E_{measured}$	E_{calc} Exp. (GPa)		E_{calc} Theory		$\sigma_{0.2\%}$	RSS Super	RSS Ordinary	RSS Reference Values	
[$\bar{4}$43]	207	206	206	182	220	-216	76	52		
[$\bar{3}$61]	163,157, 159	165	165	134	148	-188,-185 +180	94	61	98	
[$\bar{3}$715]	175,170	169	169	173	157	-131 +130	65	36		68
[$\bar{1}$55]	222	202	201	205	206	----	N/A	N/A		
Refs.		[1]	[2]	[3]	[2]				[4]	[5]

[1] Y. He, R. B. Schwarz, A. Migliori, and S. H. Whang, *J. Mater. Res.*, **10,** 1187 (1995).
[2] K. Tanaka, T. Ichitsubo, H. Inui, M. Yamaguchi, and M. Koiwa, *Phil. Mag. Lett.*, **73,** 71 (1996).
[3] C. L. Fu and M. H. Yoo, *Phil. Mag. Lett.*, **62,** 159 (1990).
[4] H. Inui, M. Matsumuro, D.-H. Wu, and M. Yamaguchi, *Phil. Mag. A*, **75,** (1997).
[5] M. A. Stucke, D. M. Dimiduk, and P. M. Hazzledine, MRS Symp. Proc., **288**, 471 (1993).

[$\bar{1}$55] specimen fractured during loading in the elastic region, but appreciable plastic tensile strain was realized in the other two specimens. The [$\bar{3}$ 7 15] sample was monotonically loaded in tension to approximately 1% strain before it failed; the $\sigma_{0.2\%}$ was found to be 130 MPa on this curve. The stress-strain curve obtained from the [$\bar{3}$61] specimen, which was cycled first in compression, then in tension, displayed more scatter but yielded at a stress of $\sigma_{0.2\%}$ = 180 MPa. These latter two tests are extremely encouraging because they report measurements of the tensile yield strength of single crystal γ-TiAl high temperature microsample tensile tests. The Young's modulus and resolved shear stresses for these tests are included in Table II.

The elastic properties measured from the microsample tests in fig. 9 have been compared with and found to be in good agreement with those reported in the literature. The measured values of the Young's modulus that are listed in Table II have been taken directly from the stress-strain curves. Reference values of E for each of the test orientations have been calculated from the stiffness matrices that have been determined by ultrasonic measurements and first-principles calculations. Comparisons with the experimental work of He *et al.* and Tanaka *et al.* and the theoretical calculations of Manh *et al.* are very encouraging. The agreement between the microsample measurements and the values reported in the literature has been taken as an additional sign of the validity of the microsample tests.

The 0.2% flow stress for the tension and compression tests shown in fig. 9 are listed in Table II. These values have been multiplied by the appropriate Schmid factors, and the RSS for both ordinary and superdislocation motion are also listed in Table II. For the three orientations tested in this study, the Schmid factor for superdislocation motion was greater than that for ordinary dislocation motion. Although the data does not collapse to one critical resolved shear

stress (CRSS), the RSS for superdislocations is in good agreement with the reference values for crystals tested at approximately the same orientations, see for example and Inui et al for the [361] orientation and Stucke et al. for the [$\bar{3}$ 7 15] orientation. Moreover, TEM studies of deformed single crystals have reported the prevalence of superdislocation activity. In light of these observations, it has been concluded that superdislocation are also responsible for the plastic deformation obtained from the microsample experiments. The observed violation of Schmid's law is in agreement with what has been reported in the literature.

The tension and compression yield strengths for the [$\bar{3}$ 7 15] orientation can both be drawn from the data in Table II. Comparison of the data, which was obtained in two separate tests, suggests that the tension-compression asymmetry at 300K and 500K is very small. A complete cyclic loading experiment that has been conducted to measure the tension-compression asymmetry of the yield strength on the same specimen is shown in fig. 10. Predictions based on the asymmetrical dissociation of superdislocations in TiAl suggests that a strong difference between the tensile and compressive flow stresses should exist when the cross-slip locking of superdislocations controls deformation. Figure 10 shows results from a [$\bar{3}$61] test at 500K, in which a sample was yielded to slightly beyond the 0.2% flow stress and then unloaded and subsequently reloaded, this time in tension, until it yielded a second time. For this test, the compressive flow stress was measured to be -185 MPa, and the comparable value for tension was found to be +180 MPa.

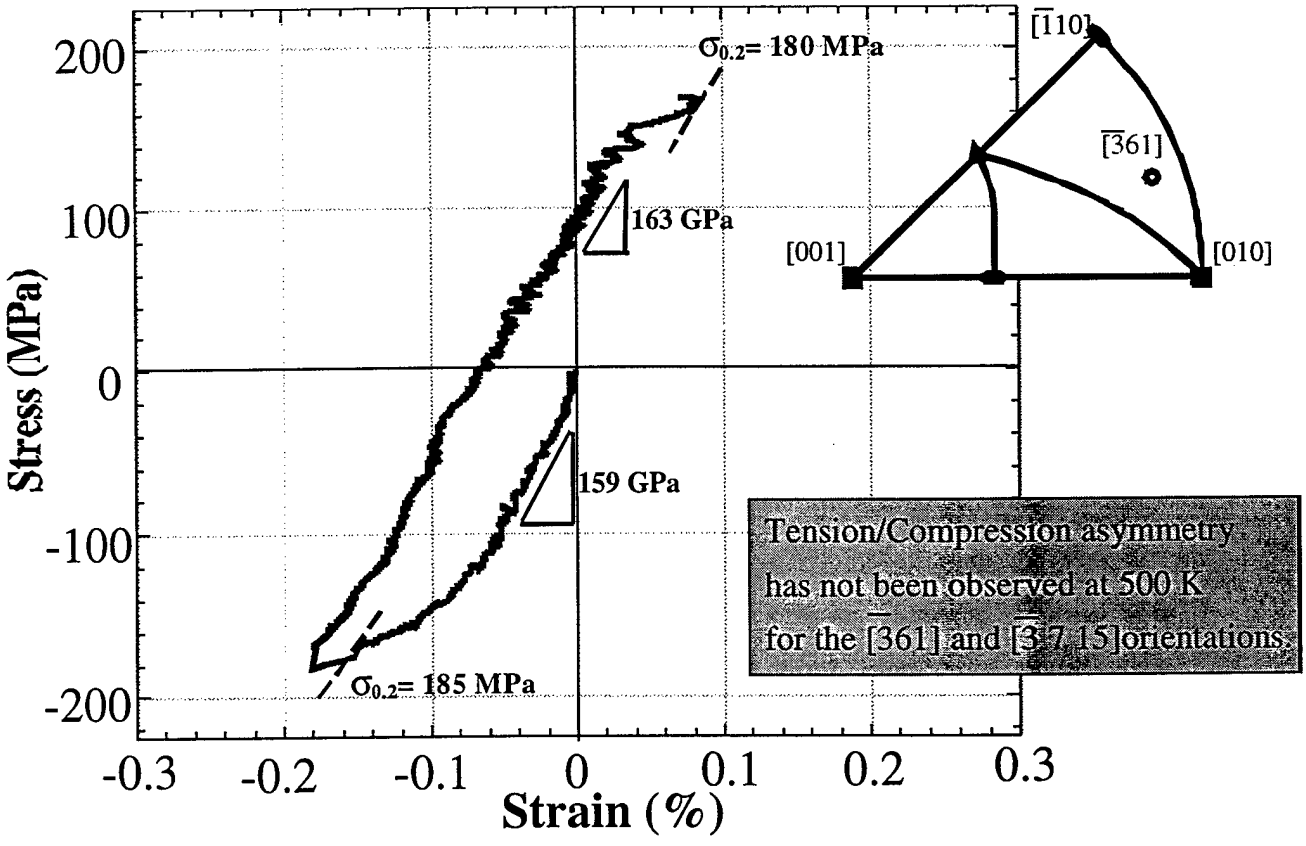

Fig. 10: Stress-strain curves for the cyclic loading of a single crystal oriented along the [$\bar{3}$61] direction and tested at 500K. The sample was pushed until it yielded in compression ($\sigma_{0.2\%}$= -185 MPa) then pulled until it yielded in tension ($\sigma_{0.2\%}$= +180 MPa).

These preliminary test results indicate that the tension-compression asymmetry of the yield strength is negligible for the temperatures and orientations tested. A plot of compressive flow stresses for single crystal tests performed by Inui *et al.*, at orientations within ~5• of the $[\bar{3}61]$ orientation tested in this work, is displayed in fig. 11. The fact that the microsample data overlays the compression curves attests to the validity of the experiments, and the shape of the $\sigma_{0.2\%}$ versus temperature curves provides a possible explanation for the absence of a tension-compression asymmetry at 500K. The temperature of the cyclic loading test performed for the $[\bar{3}61]$ orientation lies below the temperature at which anomalous yielding is observed. Further testing at higher temperatures and at a variety of orientations is needed to fully explain the tension-compression asymmetry and its relation to cross-slip locking in γ-TiAl.

Preliminary results have been obtained from single crystal tension tests performed on Ti-52Al at 500K. Individual grains were oriented using only back reflection Laue, and the exact tensile axis of each of the samples could not be determined. Figure 12 displays stress - strain curves for two tensile samples cut from the same grain at the same orientation. The tests resulted in a $\sigma_{0.2\%}$ = 180 and 173 MPa and a Young's modulus of E = 201 and 187 GPa. Comparison of these values with those measured on similar orientations of Ti-56Al at the same temperature shows a small variation in the flow stress and Young's modulus. Microstructural observations and additional tests on Ti-52Al are in progress.

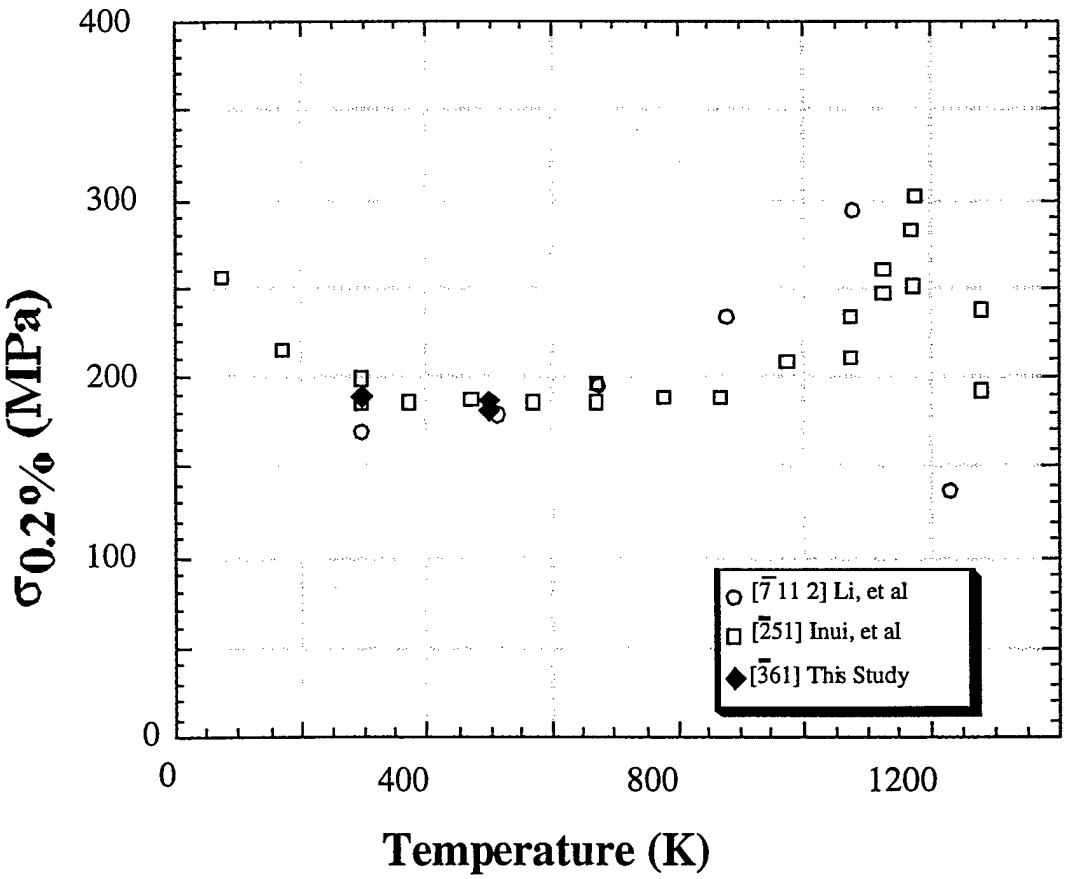

Fig. 11: Experimentally measured values of $\sigma_{0.2\%}$ as a function of temperature for near $[\bar{3}61]$ oriented crystals. The tensile and compressive yield strengths measured in this study are both in good agreement with the compressive data that have been reported by Li and Whang (*Mater. Sci Eng.*, **A152**, 182, 1992) and Inui *et al.*

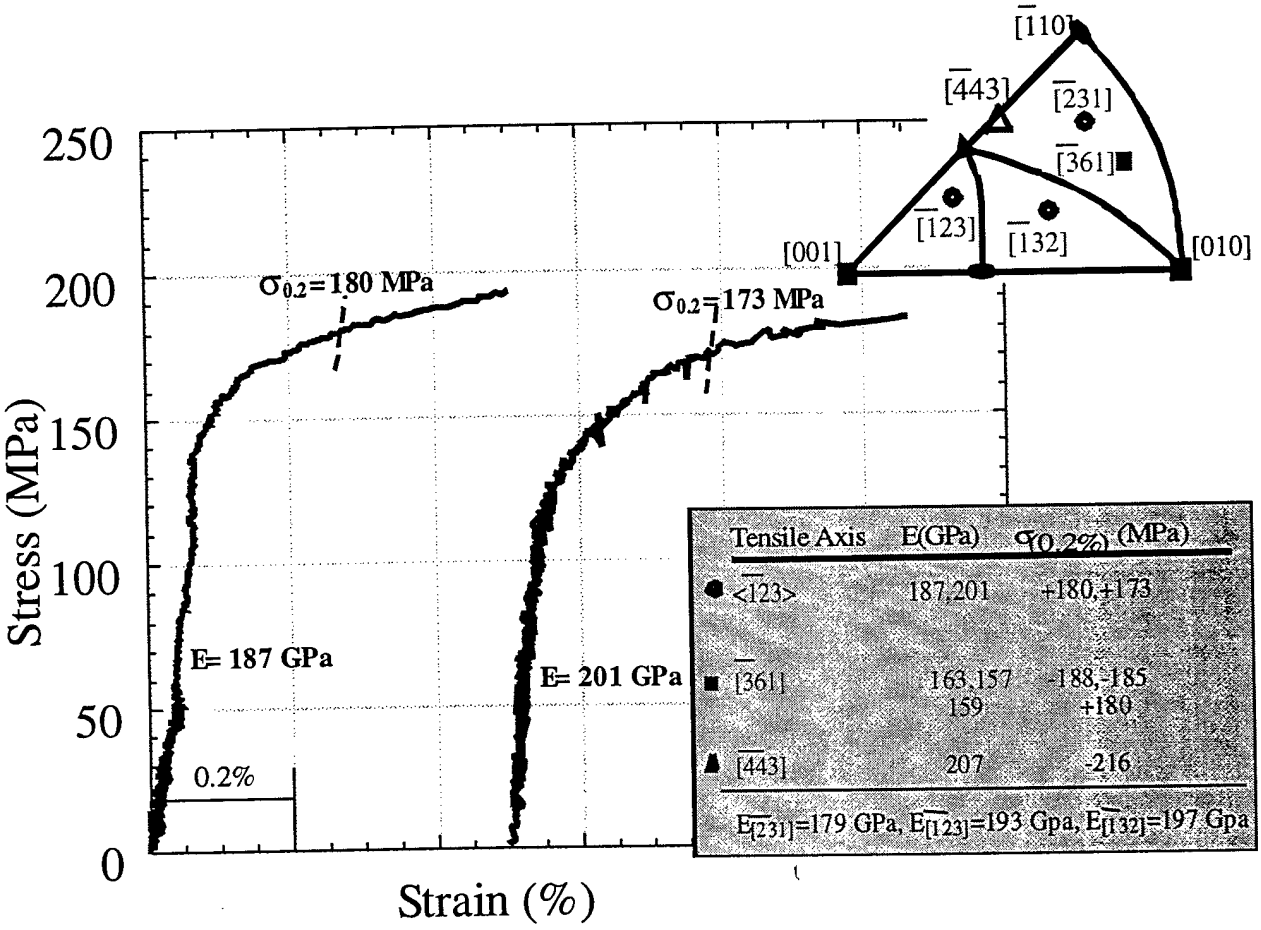

Fig. 12: Tensile stress strain curves for single crystal Ti-52Al at 500K. The extended standard triangle is shown, displaying the possible specimen orientations. Comparison is made with tests performed on Ti-56Al at the same temperature and similar orientations.

As part of the current project, we have also taken the original microsample tester design of Sharpe and increased its testing capabilities with extensive modifications. A large thrust in the redesign and construction of the next-generation microsample test machine has focused on improving its user interface. Loading on the new machine is accomplished through the use of a piezo-electric actuator and is measured with a 20 pound load cell. This actuator has a full feedback control loop, allowing for very precise load or stroke controlled loading of the microsamples during testing. It is controlled with LabView software, which expands the ability of the tensile tester to include creep testing as well as cyclic tension-tension and tension-compression experiments. A picture of the new system, displaying all of its components, is given in fig. 13.

Sharpe's original ISDG strain measurement system has been enhanced, and a parallel system that measures grip displacement with a high resolution capacitance gage has been added for high strain measurements. The improvements in the ISDG are related to the integration of LabView software, enhanced computer processing capabilities and improvements in the signal to noise ratio. The interference fringe patterns, which are the basis of the ISDG technique, were previously tracked separately, but with the new system the phase of the entire pattern is

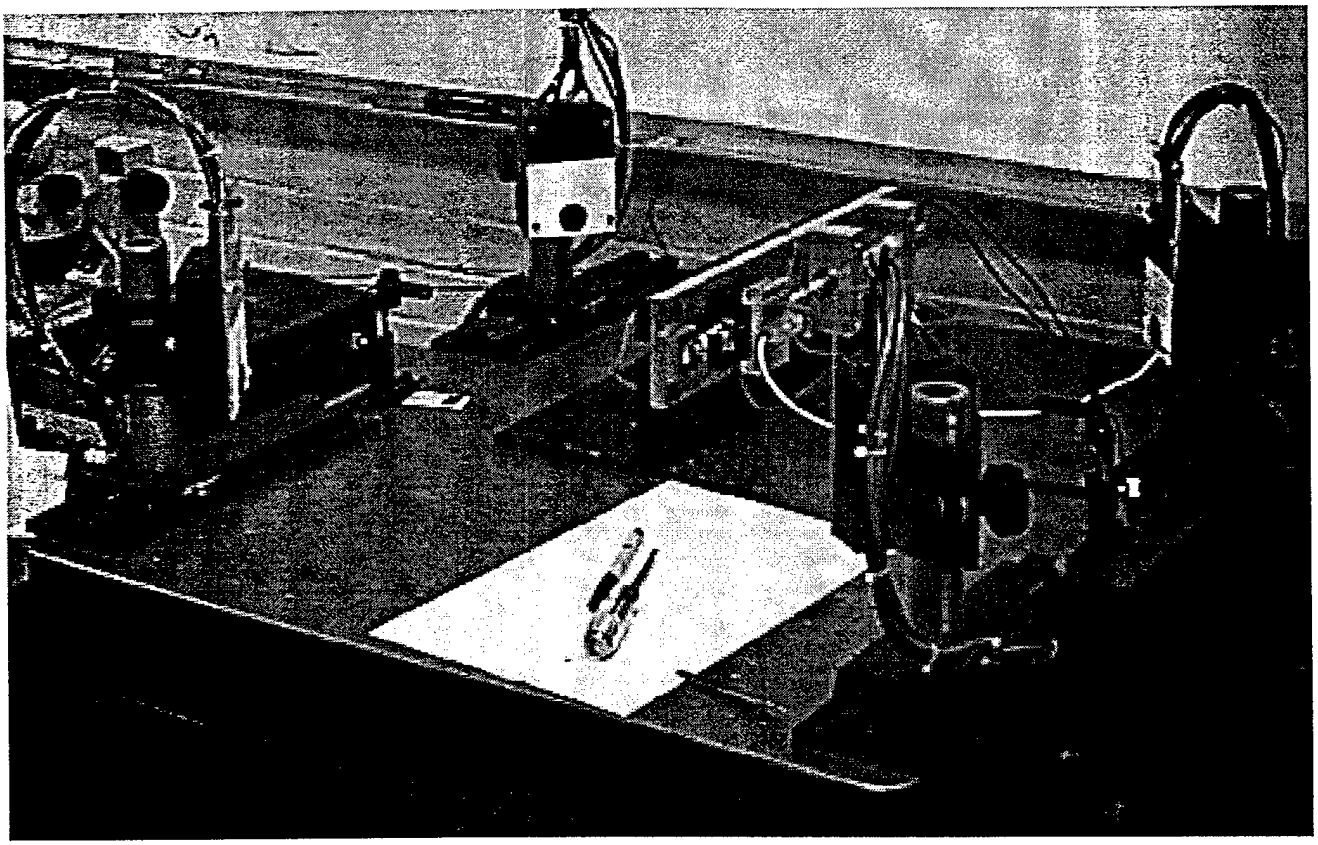

Fig. 13: The microsample testing system at The Johns Hopkins University.

monitored by inputting the fringe pattern into the LabView software and performing real-time Fourier transforms. Measuring the phase shift of the fringe pattern, which is proportional to the strain in the sample, reduces the scatter in the optical fringe signals and greatly simplifies strain measurement with the ISDG. The ability to perform tests in a lighted room has been added by the use of a narrow band-pass filter that allows transmission of the laser wavelength and eliminates all other white light. The signal to noise ratio of the system has been greatly improved by using these filters, by increasing the sensitivity of the diode arrays, and by using brighter diode lasers with adjustable intensities.

2. PERSONNEL SUPPORTED :

- Associate Professor Kevin J. Hemker ;*PI*, AFOSR supports 1 month salary per year
- Dr. Mukul Kumar ; *postdoctoral fellow*, supported 50% AFOSR / 50% NSF
- Mr. John Balk ; *Ph.D. graduate student, M.S received 1997*, with JHU Whiting School of Engineering Materials Fellowship.
- Mr. Marc Zupan ; *Ph.D. graduate student , M.S received 1997.*

3. PUBLICATIONS RELATED TO THIS GRANT :

Dissertations:

1. Thomas John Balk, "Relating Mechanical Properties and Dislocation Cores in the $L1_2$ Intermetallic System Ni_3Ge-Fe_3Ge", Masters Essay, Johns Hopkins University, Baltimore MD 21218, (1997).
2. Marc Zupan, "Measurement of the Mechanical Properties of Single Crystalline Gamma Ti-55.5%Al", Masters Essay, Johns Hopkins University, Baltimore MD 21218, (1997).

(These dissertations can be obtained by placing a request with The Johns Hopkins University Library, Special Collections Department, 410-516-8348)

Journal Articles:

1. K.J. Hemker, "Correlating Dislocation Positions with Intensity Peaks in Weak-beam TEM Images", *Phil Mag. A*, **76**, pp 241-265, (1997).
2. Mukul Kumar and K.J. Hemker, "Characterization of dislocation structures associated with small-angle boundaries in annealed $L1_2$ Ni_3Ge", *Phil Mag. Letters*, **76**, pp 399-407, (1997).
3. M. Zupan and K.J. Hemker, "Tensile/compressive properties of single crystal gamma Ti-55.5% Al", *Metallurgical and Materials Transactions*, **29A**, pp 65-71, (1998).
4. Ping Wang, Mukul Kumar, K.J. Hemker and Vijay K. Vasudevan "Characterization of Unusual Stacking Faults and Dislocations in the Massive Gm Phase in a Quenched Ti-46% Al Alloy", *Materials Letters*, **35** (5-6), pp 283-289, (1998).
5. Mukul Kumar and K.J. Hemker, "Dislocation core dissociations in the intermetallic Al_3Ti", *J. of Materials Research*, **13** (5), pp 610-624, (1998).
6. T.J. Balk, Mukul Kumar and K.J. Hemker, "Relating alloy chemistry, dislocation cores and mechanical properties in the $(Ni_xFe_{1-x})_3Ge$ system", *Scripta materialia*, **39**, pp. 577-582 (1998).

Refereed Symp. Proceedings:

1. K.J. Hemker, Mukul Kumar and T.J. Balk, "Observing Dislocation Cores and Relating Their Structure to Macroscopic Deformation Processes", *Deformation and Fracture of Ordered Intermetallic Materials III*, Eds. Soboyejo et al., TMS Publications, pp 311-321, (1996).
2. M. Zupan, D. A. LaVan, and K.J. Hemker, "Tensile testing of single crystal gamma Ti - 55.5 Al", *MRS Symp. Proc.*, **460**, pp 171-176 (1997).
3. T.J. Balk, Mukul Kumar and K.J. Hemker, "Relating Mechanical properties with dislocation cores in Ni_3Ge-Fe_3Ge intermetallic alloys", *MRS Symp. Proc.*, **460**, pp 641-646 (1997).
4. K.J. Hemker, Min Lu, and M. Zupan, "Deformation Processes and Dislocation Motion in Gamma-TiAl", *Structural Intermetallics*, Eds. Nathal et al., TMS Publications, pp 147-156, (1997).

5. K.J. Hemker and W.D. Nix, "Mechanisms of Dislocation Creep in Intermetallic Alloys of the Ni-Al-Ti System *Structural Intermetallics*, Eds. Nathal et al., TMS Publications, pp 21-32, (1997).

4. CONFERENCE PRESENTATIONS RELATED TO THIS GRANT :

1996 International Conference on TEM of Intermetallic Alloys, Birmingham, ENGLAND

- "Difficulties associated with observing dislocation cores in intermetallic alloys and the need for image simulations.", *Hemker.* (Invited)

1996 AFOSR Workshop on High Temperature Materials, Bangor ME

- "Promoting atomic scale engineering by quantifying experimental observations of dislocation cores" *Hemker*, Kumar, Balk, and Zupan. (Invited)

1996 Fall TMS Conference, Cincinnati OH

- "Observing dislocation cores and relating their structure to macroscopic deformation processes", *Hemker*, Kumar and Balk. (Invited)

1996 MRS Fall Meeting, Boston MA

- "Tensile testing of single crystal gamma Ti - 55.5 Al", Zupan, LaVan and Hemker.
- "Relating Mechanical properties with dislocation cores in Ni_3Ge-Fe_3Ge intermetallic alloys", *Balk*, Kumar and Hemker.

1997 Winter Annual TMS Conference, Orlando FL

- "Tensile/compressive properties of single crystal gamma Ti-55.5% Al, *Zupan* and Hemker.

Second International Symposium on Structural Intermetallics, September 1997

- "Dislocation motion and deformation processes in gamma TiAl", Hemker, *Lu* and *Zupan*.
- "Dislocation core structures in the intermetallic alloy $(ni_x,Fe_{1-x})_3Ge$", *Balk*, Kumar and Hemker.

1997 Fall TMS Conference, Cincinnati OH

- "Characterizing Superdislocations in $L1_2$ Structures with TEM Observations and Image Simulations: Examples with APB- and SISF Dissociations", *Kumar* and Hemker.
- "Correlating Yielding Behavior with Dislocation Core Structures in Ni_3Ge-Fe_3Ge Intermetallic Alloys", *Kumar* , Balk and Hemker.

1997 MRS Fall Meeting, Boston MA

- "Measurement of Fault Energies in Ni_3Ge-Fe_3Ge Intermetallic Alloys, Kumar, Balk and *Hemker*.

1998 Winter Annual TMS Conference, San Antonio TX

- "Relating alloy chemistry, dislocation cores and mechanical properties in the $(Ni_xFe_{1-x})_3Ge$ system", Balk, Kumar and Hemker.